

# 2D Radiative Casson-Carreau Hybrid Nanofluid Flow through a Circular Cylinder in a Darcy-Forchheimer Porous Medium



Ahmed M. Rashad<sup>1</sup>, Mohamed A. Nafe<sup>2\*</sup>, Dalia A. Eisa<sup>2</sup>

<sup>1</sup> Department of Mathematics, Faculty of Science, Aswan University, Aswan, 81528 Egypt.

<sup>2</sup> Department of Mathematics, Faculty of Science, New Valley University, Al-Wadi Al-Gadid, 72511 Egypt.

doi: [10.21608/nujbas.2023.218751.1012](https://doi.org/10.21608/nujbas.2023.218751.1012)

## Abstract

The impulse back the sitting treatise is to study the properties of magnetohydrodynamic flow and heat transfer for Casson-Carreau hybrid nanofluid under the effects of heat sink/source, magnetic field, thermal radiation and slip conditions in a Darcy-Forchheimer porous medium with injection/suction effect. The examined hybrid nanofluid includes rheological action of non-Newtonian and pursues fluid paradigm of Casson-Carreau considering water as a base fluid, whereas Aluminium oxide and Copper as a hybrid nanoparticles. In this model, the formularization of the Casson-Carreau hybrid nanofluid has been used for expressing boundary layer problem. The obtained differential equations are switched by using non-similar transformations and then solved numerically. Some of the outcomes of the examination in both Casson-Carreau models influence the upsurging transfer of heat by thermal radiation and blowing/suction parameters. Moreover, skin friction coefficient display identical behaviour for thermal radiation, but the opposite behaviour is noticed in the state of the suction/injection parameter.

**Keywords:** Hybrid nanofluid; Circular cylinder; Thermal radiation; Injection/suction; Heat source/sink.

## 1. Introduction

Many flow properties in modernistic engineering are not intelligible using the type of Newtonian fluid. As a result, non-Newtonian fluid theory has proved helpful. Casson and Carreau fluids are two of these fluids. Fluids of Casson and Carreau are categorized as the most widely used non-Newtonian fluids, which have numerous uses in processing of food, bioengineering, operations of digging and metallurgy. For portending the flow demeanor of tincture-oil hangs, Casson [1] introduced paradigm of Casson fluid. The concentration, temperature and velocity for convection nanofluid flow with gravity-driven via a wiggling perpendicular sheet in a porous system with magnetic field effect were analysed by Kataria and Mittal [2]. The impacts of Dufour, radiative and dissipation on magneto-Casson fluid flow with free convective across a columnar permeable sheet were discussed by Rajakumar et al. [3]. Magnetohydrodynamic (MHD) double-diffusive flow of Casson deliquescent in a non-Darcian porous material with effects of thermodiffusion and Newtonian heating is investigated by Seth et al. [4] considering the key parameters of Casson liquid flow characteristics. In this respect, very newly Mittal and Patel [5] studied motion of Brownian and thermophoresis on flow of two-dimensional (2D) crossbred convection MHD Casson fluid with heat source and thermal radiation. El-Zahar et al. [6] examined time-dependent Casson flow with MHD mixed convection in the stagnation point of an impulsively spinning sphere.

Using Carreau kind, a lot of scholars have looked into and investigated a diverse range of biological and industrial flow problems. For example, the action of slanted MHD Carreau fluid filled with nanoparticles in 2D channel was examined analytically by Akram [7]. Hayat et al. [8] used the model of Carreau to explore the convection of mixed impact on wavy flow of nanofluid, discovering that the number of Weissenberg and index of energy law affect inversely on shear stress. Vajravelu et al. [9] published a research on Carreau model across the phenomena of peristaltic with environment of magnetic and slip velocity using theory of perturbation on tiny amplitudes of number of Weissenberg and confirmed that velocity slip extending the volume of bolus. Kothandapani

et al. [10] conducted research on peristaltic flow for Carreau model conductive electrically in porous materials along a tapered conduit. They found that Carreau fluid estimated high pressure than Newtonian fluid in 2D channel. Newly, several authors [11-16] investigated non-Newtonian fluid flows in various geometrical models.

Owing to multiple technical and engineering applications, it is significant to grasp and explore the flow of MHD. MHD convective flow of the visually thick nanofluid via a perpendicular oscillating surface with the action of radiation was assayed by Kataria and Mittal [17]. Raghunath et al. [18] recently found mass and heat transfer on MHD non-Newtonian fluid flow via an infinite porous vertical surface. The convection of MHD hybrid nanoliquid (Al<sub>2</sub>O<sub>3</sub>-Cu/Water) with interior heat absorption/generation in a sloping porous bore was checked by Chamkha et al. [19]. Actions of Hall current, chemical reaction, thermal radiation and heat absorption on convective MHD flow over a permeable sheet were discussed by Obulesu et al. [20]. Flow of free convection of an unsettled MHD nano-fluid in a sloping square bore including a heated circular hurdle was investigated by Mansour et al. [21]. Also, it has been discovered that Nusselt number is shown to be sensitive to size of the central obstruction and it decreases enough as the inner cylinder radius grows. Abdelhafez et al. [22] studied mixed convection of MHD hybrid nanofluid flow via a stretching and shrinking permeable plate embedded in a porous system. Actions of yield stress and chemical reaction on magnetic 2-phase nanoliquid flow in a porous regime with thermal ray were checked by Abdelhafez et al. [23].

The present paper has comparison of two diverse kinds of non-Newtonian hybrid nanofluids: Casson-Carreau paradigm under different key parameters.

## 2. Formulation and Physical Model

Time-independent MHD natural heat transfer convection flow from the horizontal circular cylinder of Carreau-Casson hybrid nanofluid is investigated. Fig. 1 depicts the model of flow and associated coordinate regime.  $B_0$  is the strength of magnetic field, which is typically applied to the flow. The coordinate of  $x$  is pinpointed via the horizontal cylinder diameter from the least point and the  $y$ -axis is pinpointed normal to the plate. Regarding the vertical  $0 \leq \phi \leq \pi$  and the trend angle of  $y$ -axis is  $\phi = x/a$ . With rev of gravity, the  $g$  works down. Initially, both the horizontal cylinder and fluid are kept at the same temperature. They are immediately raised to a temperature  $T_w > T_\infty$ , it is the ambient warmth of the fluid that remains unconverted.

Tensor of stress is known as for Carreau fluid

$$\bar{\tau}_{ij} = \eta_0 \left[ 1 + \frac{(n-1)}{2} (\Gamma \bar{\gamma})^2 \bar{\gamma}_{ij} \right], \tag{1}$$

where  $\bar{\tau}_{ij}$ ,  $\eta_0$ ,  $\Gamma$  and  $n$  are refer to the supplemental tensor of stress, viscosity of zero shear average, value of time and power-law indicator, respectively.

$$\text{Where } \bar{\gamma} = \sqrt{\frac{1}{2} \sum_i \sum_j \bar{\gamma}_{ij} \bar{\gamma}_{ij}} = \sqrt{\frac{1}{2} \Pi}, \tag{2}$$

fluid of Casson have 2D steady flows presented by (see Ref. [24])

$$\tau_{ij} = \begin{cases} 2 \left( \mu_B + \frac{p_y}{\sqrt{2\Pi}} \right) e_{ij}, & \Pi \geq \Pi_c \\ 2 \left( \mu_B + \frac{p_y}{\sqrt{2\Pi_c}} \right) e_{ij}, & \Pi < \Pi_c \end{cases}, \tag{3}$$

the second strain tensor invariant is  $\Pi$ . Depending on the above assumptions, the controlling equations (see Refs. [24-26]) are:

$$\frac{\partial u}{\partial x} + \frac{\partial v}{\partial y} = 0, \tag{4}$$

$$u \frac{\partial u}{\partial x} + v \frac{\partial u}{\partial y} = \nu_{hnf} \left[ \left( 1 + \frac{1}{\beta^*} \right) \frac{\partial^2 u}{\partial y^2} + \frac{3}{2} (n-1) \Gamma^2 \left( \frac{\partial u}{\partial y} \right)^2 \frac{\partial^2 u}{\partial y^2} \right] + \frac{(\rho\beta)_{hnf}}{\rho_{hnf}} g (T - T_\infty) \sin\left(\frac{x}{a}\right) - \frac{\sigma_{hnf} B_0^2}{\rho_{hnf}} u - \frac{\nu_{hnf}}{K_1} u - \frac{C_b}{\sqrt{K_1}} u^2, \tag{5}$$

$$u \frac{\partial T}{\partial x} + v \frac{\partial T}{\partial y} = \frac{k_{hnf}}{(\rho c_p)_{hnf}} \frac{\partial^2 T}{\partial y^2} + \frac{1}{(\rho c_p)_{hnf}} \frac{16\sigma^* T_\infty^3}{3k^*} \frac{\partial^2 T}{\partial y^2} + \frac{Q_0}{(\rho c_p)_{hnf}} (T - T_\infty), \tag{6}$$

the conditions of boundary put in the natural stream and at the surface of the cylinder are

$$u = N_0 \mu_{hnf} \left( 1 + \frac{1}{\beta^*} \right) \frac{\partial u}{\partial y}, \quad v = v_w, \quad T = T_w + K_0 \frac{\partial T}{\partial y} \quad \text{at } y = 0, \left. \vphantom{u} \right\} \tag{7}$$

$$u \rightarrow 0, \quad T \rightarrow T_\infty \quad \text{as } y \rightarrow \infty,$$

here  $N_0, K_0$  and  $T_\infty$  are the parameters of slip velocity, thermal slip and free flow temperature. The case of no-slip when  $N_0 = K_0 = 0$ .

The equations of Cauchy-Riemann  $u = \partial \psi / \partial y$  and  $v = -\partial \psi / \partial x$  define the stream function  $\psi$ . Hence the equation of continuity is promptly fulfilled.

Proper dimensionless quantities are

$$\eta = \frac{y}{a} Gr^{1/4}, \quad \xi = \frac{x}{a}, \quad f(\eta, \xi) = \frac{\psi}{\nu \xi Gr^{1/4}}, \quad \theta(\eta, \xi) = \frac{T - T_\infty}{T_w - T_\infty}, \tag{8}$$

the converted equations are:

$$\xi \left( \frac{\partial f'}{\partial \xi} f' - \frac{\partial f}{\partial \xi} f'' \right) = \frac{\mu_{hnf} / \mu_f}{\rho_{hnf} / \rho_f} \left[ \left( 1 + \frac{1}{\beta^*} \right) f''' + \frac{3}{2} (n-1) We f''^2 f''' \right] + f f'' + \frac{(\rho \beta)_{hnf} / (\rho \beta)_f \sin(\xi)}{\rho_{hnf} / \rho} \theta - \left( \frac{\sigma_{hnf} / \sigma_f}{\rho_{hnf} / \rho_f} M + \frac{\mu_{hnf} / \mu_f}{\rho_{hnf} / \rho_f} K \right) f' - (1 + F_r \xi) f'^2, \tag{9}$$

$$\xi \left( \frac{\partial \theta}{\partial \xi} f' - \frac{\partial f}{\partial \xi} \theta' \right) = \frac{1}{Pr} \frac{(\rho c_p)_f}{(\rho c_p)_{hnf}} \left( \frac{k_{hnf}}{k_f} + \frac{4}{3} R \right) \theta'' + f \theta' + \frac{(\rho c_p)_f}{(\rho c_p)_{hnf}} S \theta, \tag{10}$$

the converted non-dimensional boundary conditions are:

$$f(0, \xi) + \xi \frac{\partial f(0, \xi)}{\partial \xi} = f_w, \quad f'(0, \xi) = \frac{S_f}{(1-\varphi_1)^{2.5} (1-\varphi_2)^{2.5}} \left( 1 + \frac{1}{\beta^*} \right) f''(0, \xi), \left. \vphantom{f} \right\} \tag{11}$$

$$\theta(0, \xi) = 1 + S_T \theta'(0, \xi),$$

$$f'(\infty, \xi) \rightarrow 0, \quad \theta(\infty, \xi) \rightarrow 0.$$

Where  $We = \left( \frac{\nu_f x Gr^{3/4}}{a^3} \right)^2$  refers to Weissenberg number, Grashof number defined as  $Gr = \frac{a^3 g \beta_f (T_w - T_\infty)}{\nu_f^2}$ ,  $Pr = \frac{\mu_f (c_p)_f}{k_f}$  is the factor of prandtl,  $M = \frac{a^2 \sigma_f B_0^2 Gr^{-1/2}}{\rho_f \nu_f}$  is the parameter of magnetic, the permeability  $K = \frac{a^2 Gr^{-1/2}}{K_1}$ ,  $F_r = \frac{c_b}{\sqrt{K}} a$  is the number of Forchheimer, radiation of thermal  $R = \frac{4\sigma^* T_\infty^3}{k^* k}$ ,  $S = \frac{Q_0 a^2}{(\rho c_p)_f Gr^{1/2} \nu_f}$  where  $S > 0$  refers to source of heat and  $S < 0$  symbolizes to heat sink,  $f_w = -\frac{a v_w}{\nu Gr^{1/4}}$  refers to suction when  $f_w > 0$  and injection when  $f_w < 0$ ,  $S_f = N_0 \mu_f \frac{Gr^{1/4}}{a}$  is the parameter of slip velocity and  $S_T = K_0 \frac{Gr^{1/4}}{a}$  is the parameter of thermal jump.

The number of Nusselt  $Nu$  and the coefficient of skin friction  $c_f$  are defined as:

$$c_f = \frac{a^2 \tau_w(x)}{\rho \nu^2}, \tag{12}$$

$$Nu = \frac{a q_w}{(T_w - T_\infty) k_f}, \tag{13}$$

where

$$\tau_w = \mu_{hnf} \left[ \left( 1 + \frac{1}{\beta^*} \right) \left( \frac{\partial u}{\partial y} \right) + \frac{(n-1)\Gamma}{2} \left( \frac{\partial u}{\partial y} \right)^3 \right]_{y=0}, \quad q_w = -k_{hnf} \left( \frac{\partial T}{\partial y} \right)_{y=0} - \frac{16\sigma^* T_\infty^3}{3k^*} \left( \frac{\partial T}{\partial y} \right)_{y=0}, \tag{14}$$

and hence, we obtained that

$$Gr^{-3/4} C_f = \xi f''(0, \xi) \frac{\mu_{hnf}}{\mu_f} \left\{ \left( 1 + \frac{1}{\beta^*} \right) + \frac{n-1}{2} [We f''(0, \xi)]^2 \right\}, \tag{15}$$

$$Gr^{-1/4} Nu = - \left( \frac{k_{hnf}}{k_f} + \frac{4}{3} R \right) \theta'(0, \xi), \tag{16}$$

### 3. Numerical approach

The solutions of nonlinear Eqs. (9)-(11) in locked form are not actually feasible. By using RKF45 with shooting technique, we can solve this problem with various parameters values. The action of involved different variables on the physical quantities as  $f'(\eta, \xi)$ ,  $\theta(\eta, \xi)$ ,  $Gr^{-3/4}C_f$ , and  $Gr^{-1/4}Nu$  are displayed pictorially.  $\Delta\eta = 0.01$  is the step size. We presumed a convenient value for away field boundary-condition in (11), i.e.  $\eta \rightarrow \infty$ , say  $\eta_\infty$ .

$$f'(\eta_\infty, \xi) = \theta(\eta_\infty, \xi) \rightarrow 0 \tag{17}$$

### 4. Explanations and Outcomes

Table (1) shows the formulation of hybrid nano-fluid characteristics that was used. Table (2) shows the thermophysical characteristics of the standard fluid H<sub>2</sub>O as well as the Al<sub>2</sub>O<sub>3</sub>/Cu nanoparticles. To confirm the thoroughness of the used method calculations and solutions, previous outcomes declared by Refs. [30-33] are matched with  $Gr^{-3/4}C_f$  and  $Gr^{-1/4}Nu$  of Newtonian fluid (i.e.  $n = 1$  and  $\beta^* \rightarrow \infty$ ), respectively, for diverse  $\xi$  values in the case of  $M = F_r = S_f = S_T = f_w = \varphi_1 = \varphi_2 = 0$  and  $Pr = 1.0$ . The comparison effects are abstracted in tables (3) and (4). The present findings display outstanding consistency with those obtained from the preceding literature as seen in tables (3) and (4). For ensuring that the numerical approach employed in this inquiry is reliable and accurate, we introduced in table (5) the computational values of  $Gr^{-3/4}C_f$  and  $Gr^{-1/4}Nu$  for different values of  $\varphi_1$ ,  $\varphi_2$ ,  $S_T$ ,  $F_r$ ,  $R$  and  $f_w$  in both models of Casson-Carreau.

Figs. 2 and 3 expose the impact of  $M$  and  $F_r$  on  $f'(\eta, \xi)$  for Carreau-Casson hybrid nanofluid. Since the experiences of magnetic field to be doubled, therefore component of  $f'$  seems to be lowered for Carreau-Casson cases. But, the opposite trend is observed when  $\eta > 5.2$  in fluid of Carreau. The source for this is that when the domain of magnetic is activated, it creates Lorentz forces, which resist the fluid flow. Figs. 4 and 5 reflect the contrast of  $\theta$  profile with growing Forchheimer number and magnetic field. It is detected that an increase happens in temperature with growing amounts of  $M$  and  $F_r$ . As Lorentz force influence on  $f'$  causes friction on the flux, causing great heat energy.

Figs. 6 and 7 present the effect of  $f'$  profile with  $R$  and  $K$  parameters in Carreau-Casson fluids, respectively. It is cleared that  $f'$  has growing conduct for considerable values of  $R$  but  $f'$  has diminishing conduct for increasing permeability in both cases of hybrid nanofluids as in Figs. 6 and 7. The thermal radiation boosts the transmission and development of additional heat into the flux, which aids increase the temperature as seen in Figs. 8 and 9.

Figs. 10 and 11 exhibit the effect of  $f_w$  and  $S_f$  on  $f'(\eta, \xi)$  for two models of Carreau-Casson hybrid nanofluids. It is noted that after reaching the higher value of the blowing/suction parameter, the velocity profiles decrease as the vigor of  $f_w$  increases. The outcomes indicate a decrease in temperature with progressing values of  $f_w$  and  $S_f$  as noted from Figs. 12 and 13. In reality, the expansion in increasing the velocity slip coefficient causes the temperature to drop to the surface and this may be the reason for the decreased sense of velocity.

The profiles of velocity under the action of  $S$  and  $S_T$  are portrayed when other parameters are constants in Figs. 14 and 15. Parameters  $S$  and  $S_T$  have the same effect for both Carreau-Casson fluids on  $f'(\eta, \xi)$  as explained in Figs. 14 and 15. It is evident that when  $S_T$  increases in the region of the cylinder surface, the velocity decreases consistently. As a result, increasing the value of the thermal jump parameter  $S_T$  causes the flow to decelerate and the boundary layer to cool. Also, it is discovered that the thickness of the momentum boundary layer significantly increases when  $S$  is upsurged. Figs 16 and 17 are drawn to show the characteristic of thermal profile for both fluid paradigms with  $\eta$  for diverse values of  $S$  and  $S_T$ . It is deduced that  $\theta(\eta, \xi)$  drops when  $S_T$  boosts. Increasing in  $S$  causes increment in temperature. Elevated amounts of  $S$  provide additional energy to the operating system, resulting in an increase in thermal boundary layer thickness in two models.

The schematics visualizations of the drag force conduct due to diverse amounts of  $f_w$  and  $R$  against  $\xi$  are plotted in Figs. 18 and 19. Here, we noted that  $Gr^{-3/4}C_f$  is diminished by boosting  $\xi$  and  $f_w$  parameters, but boosting in thermal radiation leads to rise in coefficient of skin friction in both Casson-Carreau paradigms. The factor of

Nusselt scheme is studied from Figs. 20 and 21 for diverse  $R$  and  $f_w$ . It can be proven that increasing value of both  $R$  and  $f_w$  parameters, number of Nusselt are raised.

### 5. Conclusion

The mathematical hybrid model for flow and heat transfer under the action of thermal radiation, heat sink/source, magnetic field and slip conditions with injection/suction in a Darcy-Forchheimer porous model on non-Newtonians hybrid nanoliquid is checked, and the major outcomes are as next:

- An improvement in parameters of heat and thermal radiation, yields enhancement in the velocity profile, while the velocity reduces for higher values of  $S_f$  and  $S_T$  parameters in both fluid models.
- The profile of  $f'(\eta, \xi)$  is reduced for higher values of  $M$ ,  $K$  and  $f_w$  parameter in Carreau-Casson fluid.
- Any boost in parameters of blowing/suction, slip velocity and thermal slip causes a lessening trend for temperature profile in two cases of fluids.
- The profile of  $\theta(\eta, \xi)$  is raising with increasing in magnetic field, permeability of porous regime, thermal radiation and heat sink/source parameters.
- In both discussed models, a raise in radiation of thermal and suction/blowing has a tendency to upsurge the heat transfer, whereas it decreases with raising in  $\xi$ .
- The number of Nusselt diminishes with greater amounts of thermal ray, but it proves against orientation when mixed convection and blowing/suction are increased in both models.

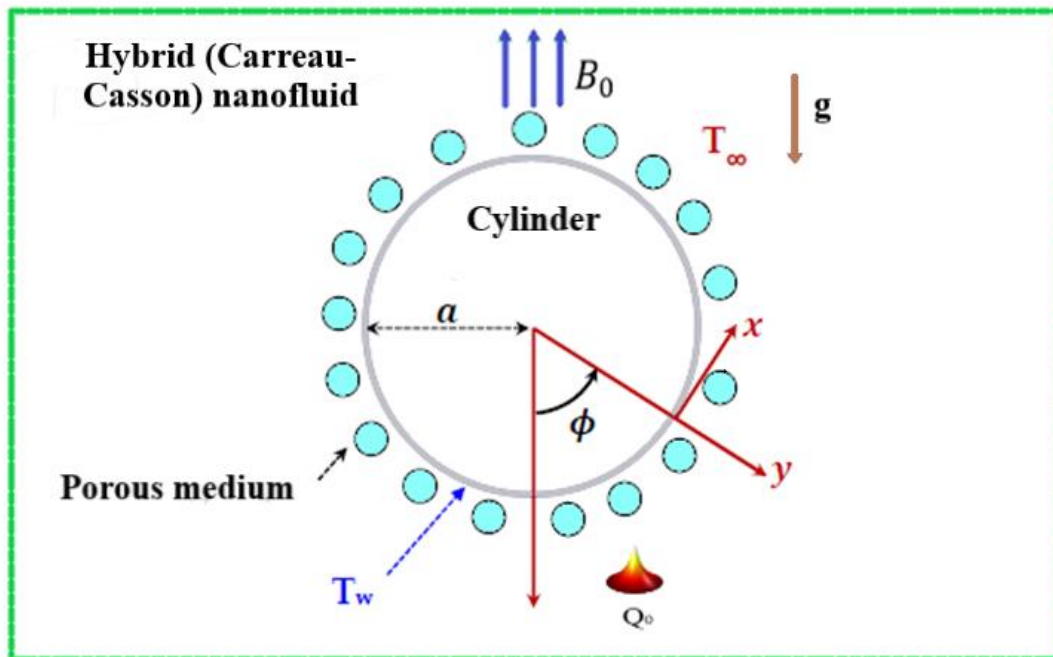


Fig. 1. The applied physical model

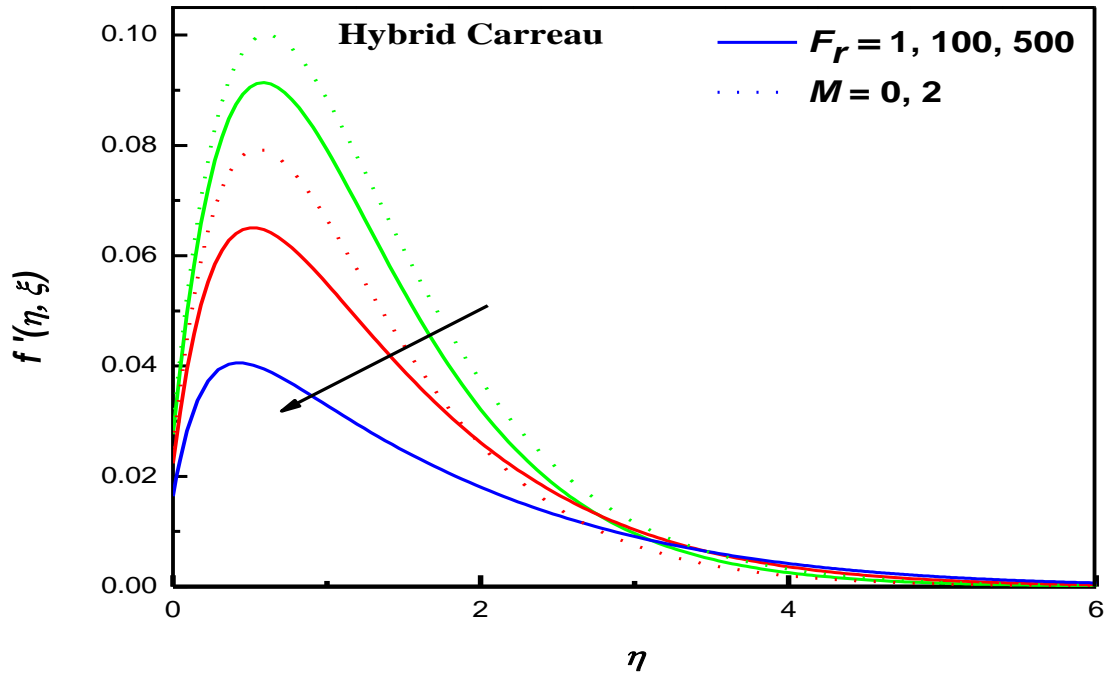


Fig. 2.  $f'(\eta, \xi)$  vs.  $F_r$  and  $M$  in Carreau case.

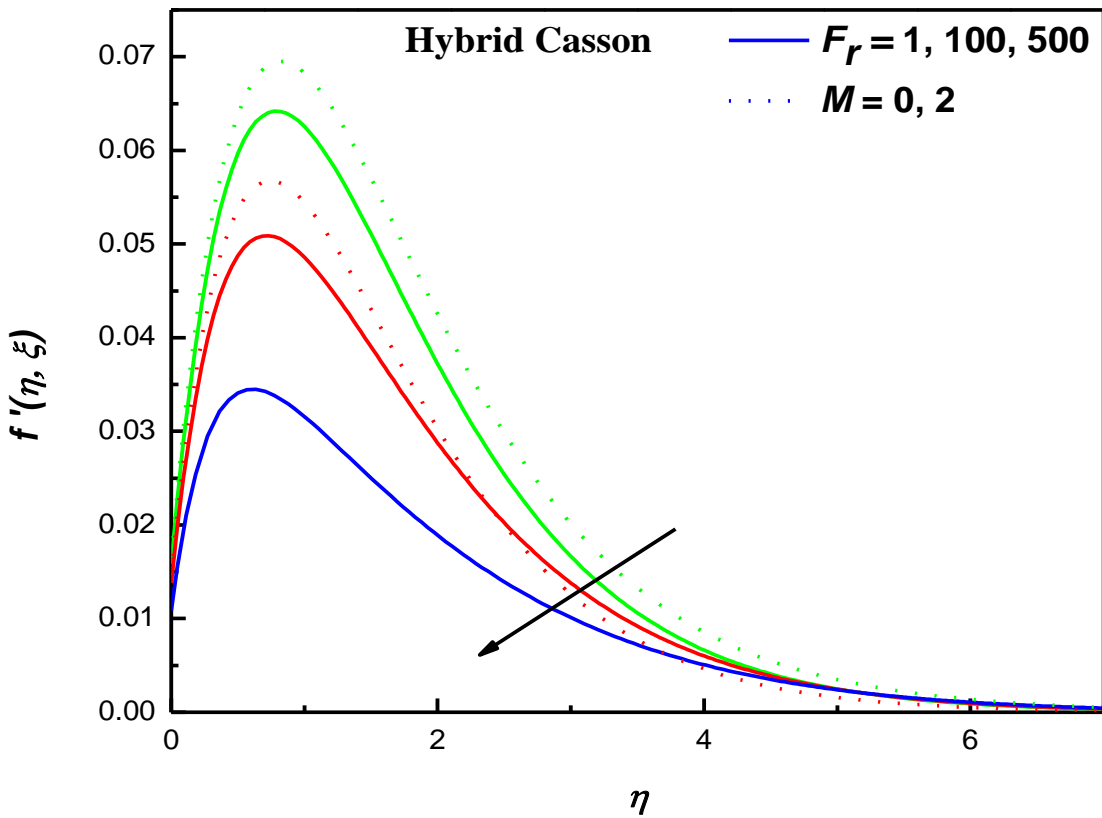


Fig. 3.  $f'(\eta, \xi)$  vs.  $F_r$  and  $M$  in Casson case.

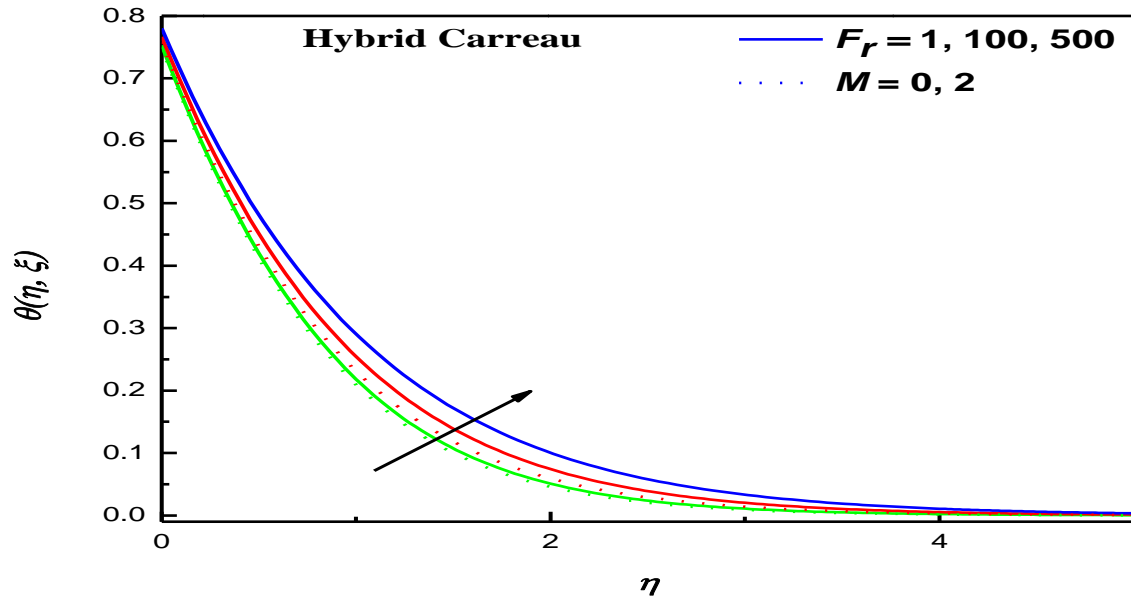


Fig. 4.  $\theta(\eta, \xi)$  vs.  $F_r$  and  $M$  in Carreau case.

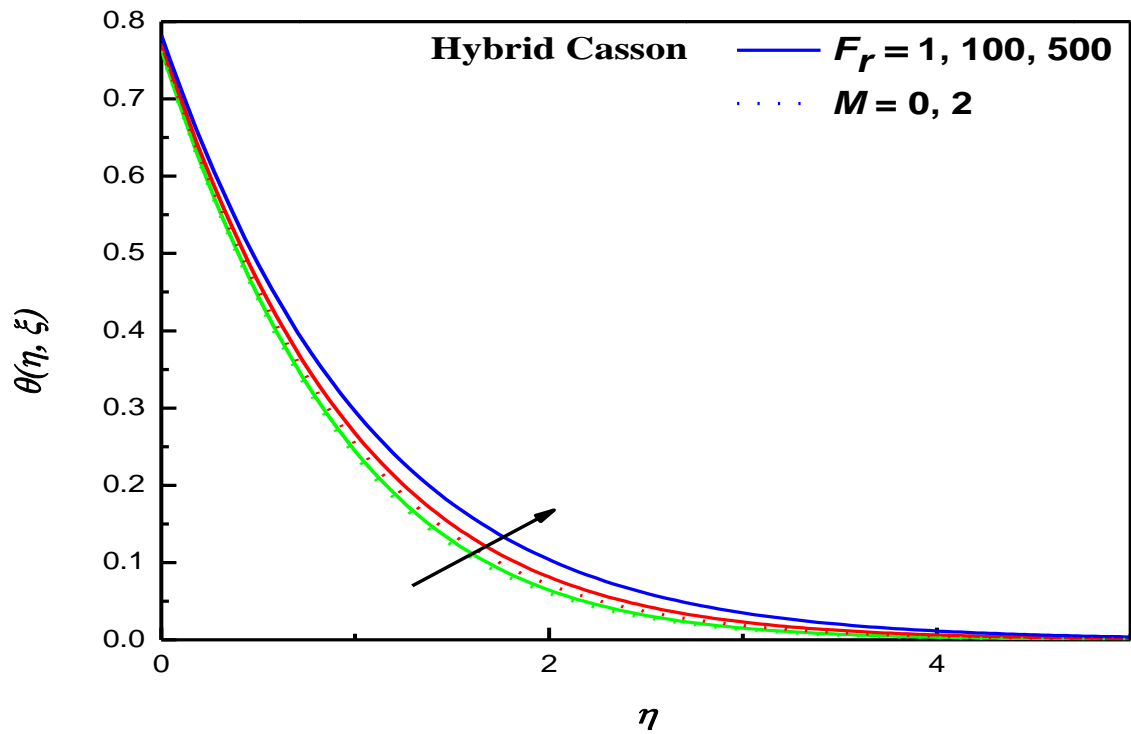


Fig. 5.  $\theta(\eta, \xi)$  vs.  $F_r$  and  $M$  in Casson case.

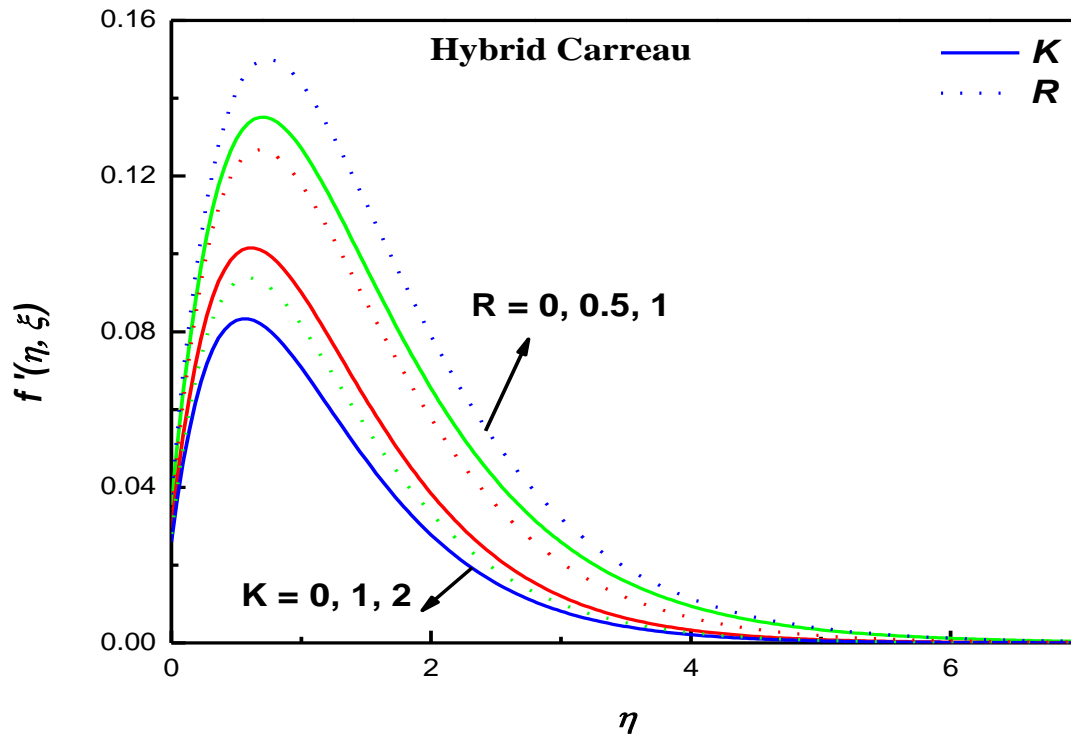


Fig. 6.  $f'(\eta, \xi)$  vs.  $R$  and  $K$  in Carreau case.

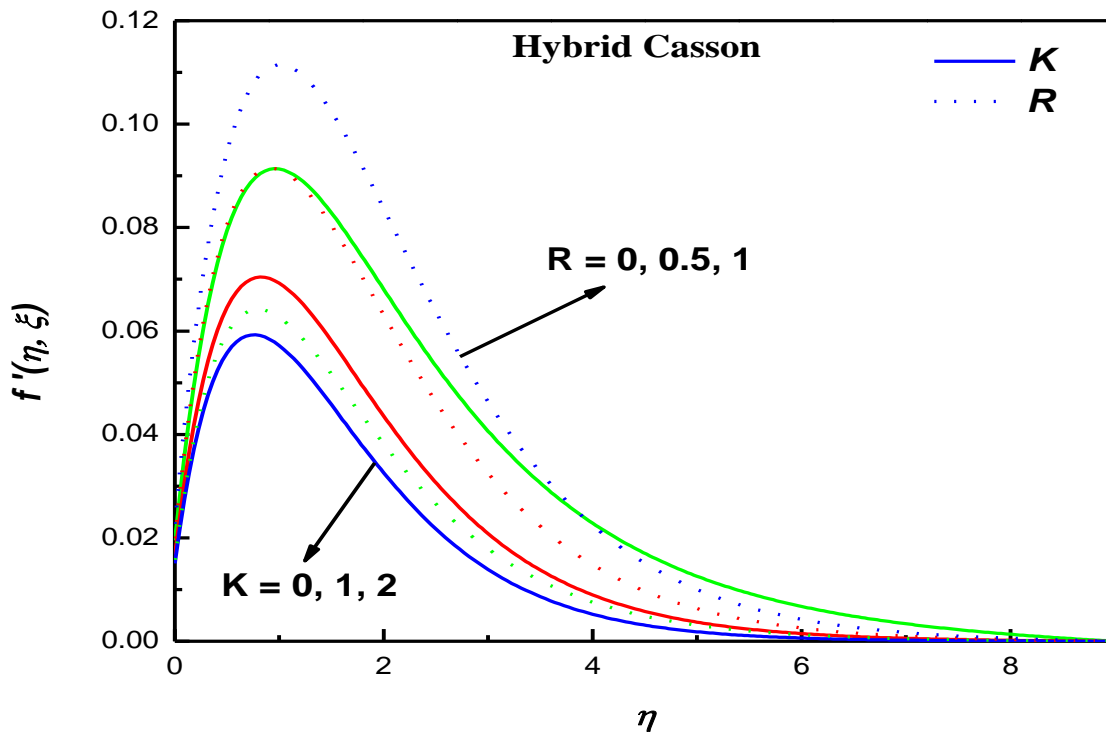


Fig. 7.  $f'(\eta, \xi)$  vs.  $R$  and  $K$  in Casson case.

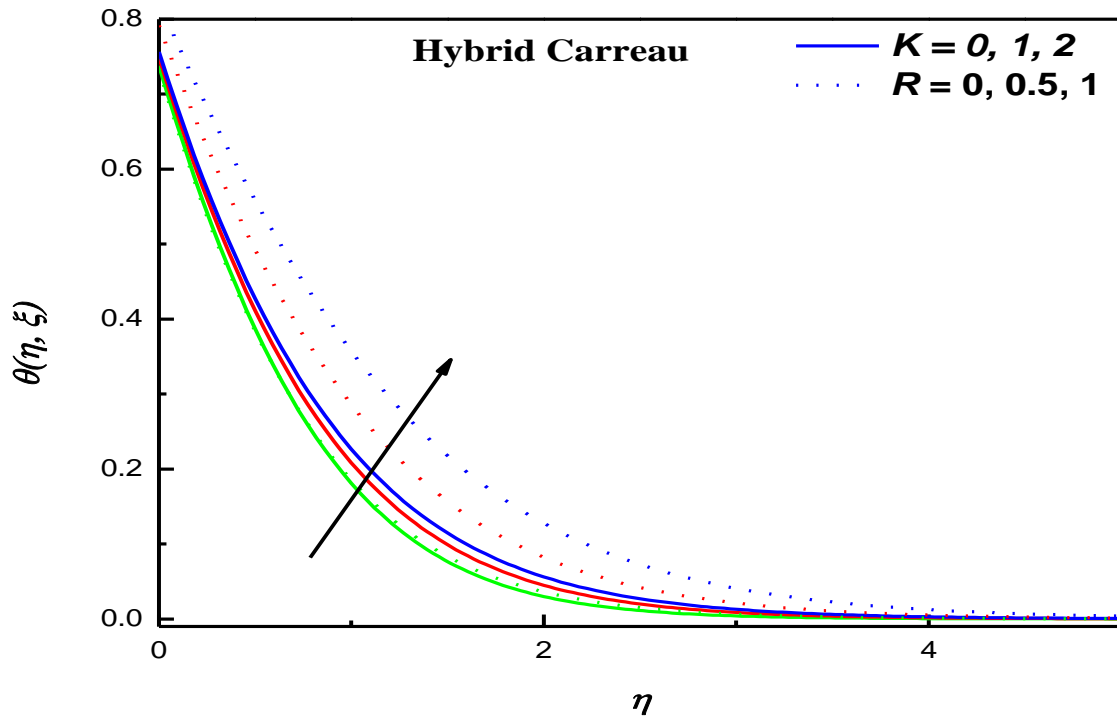


Fig. 8.  $\theta(\eta, \xi)$  vs.  $R$  and  $K$  in Carreau case.

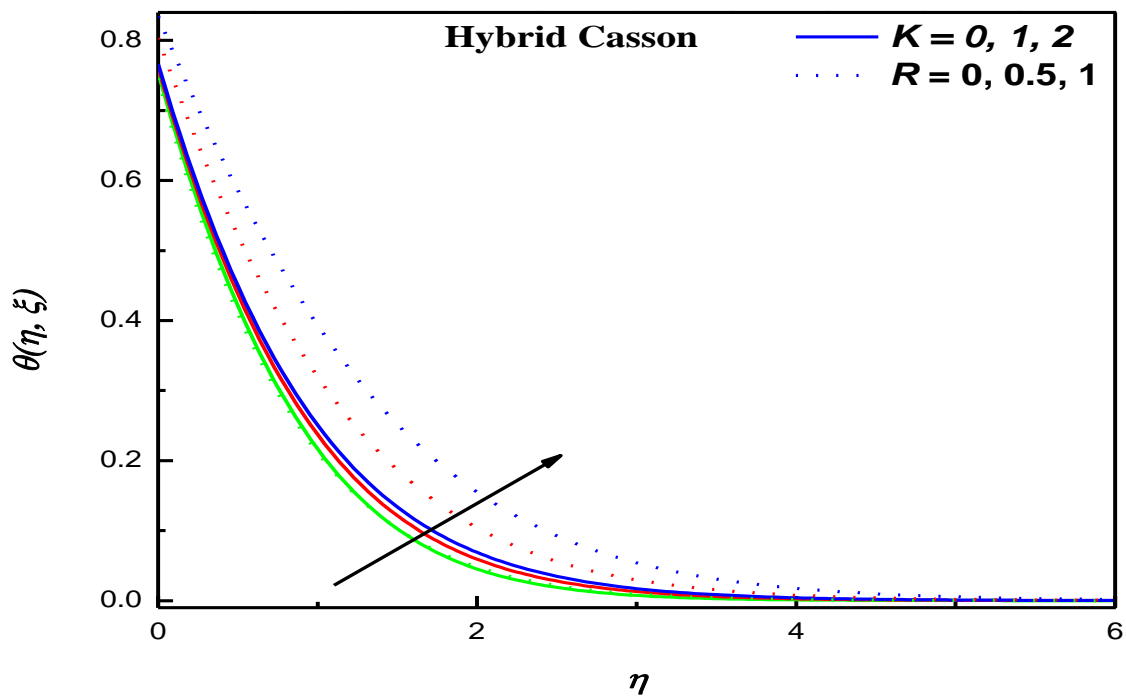


Fig. 9.  $\theta(\eta, \xi)$  vs.  $R$  and  $K$  in Casson case.

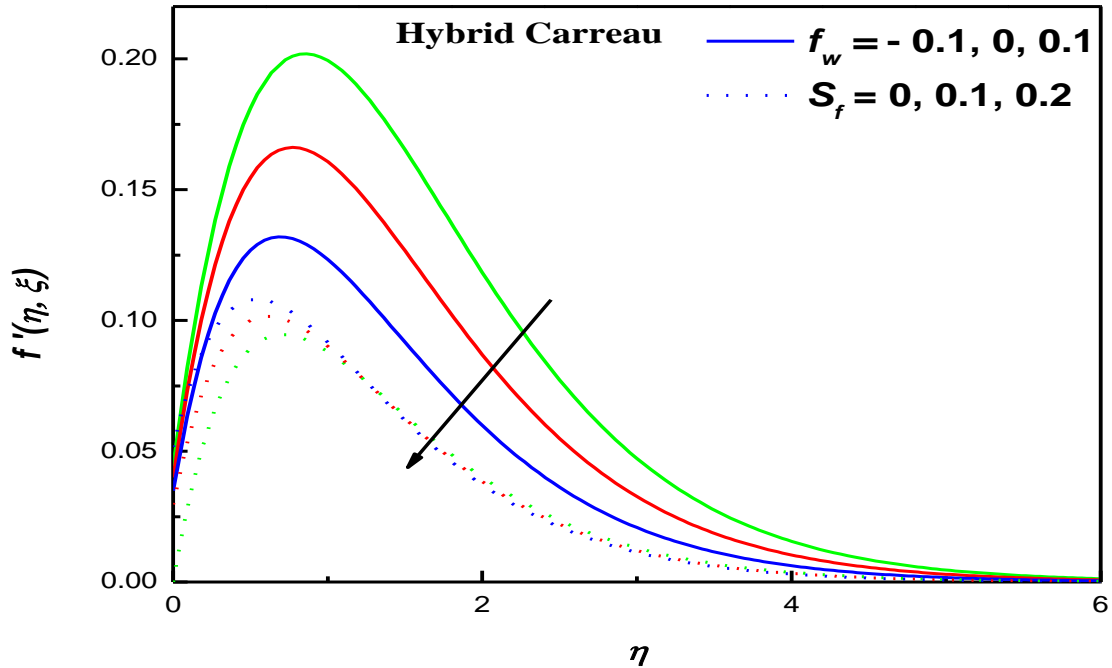


Fig. 10.  $f'(\eta, \xi)$  vs.  $f_w$  and  $S_f$  in Carreau case.

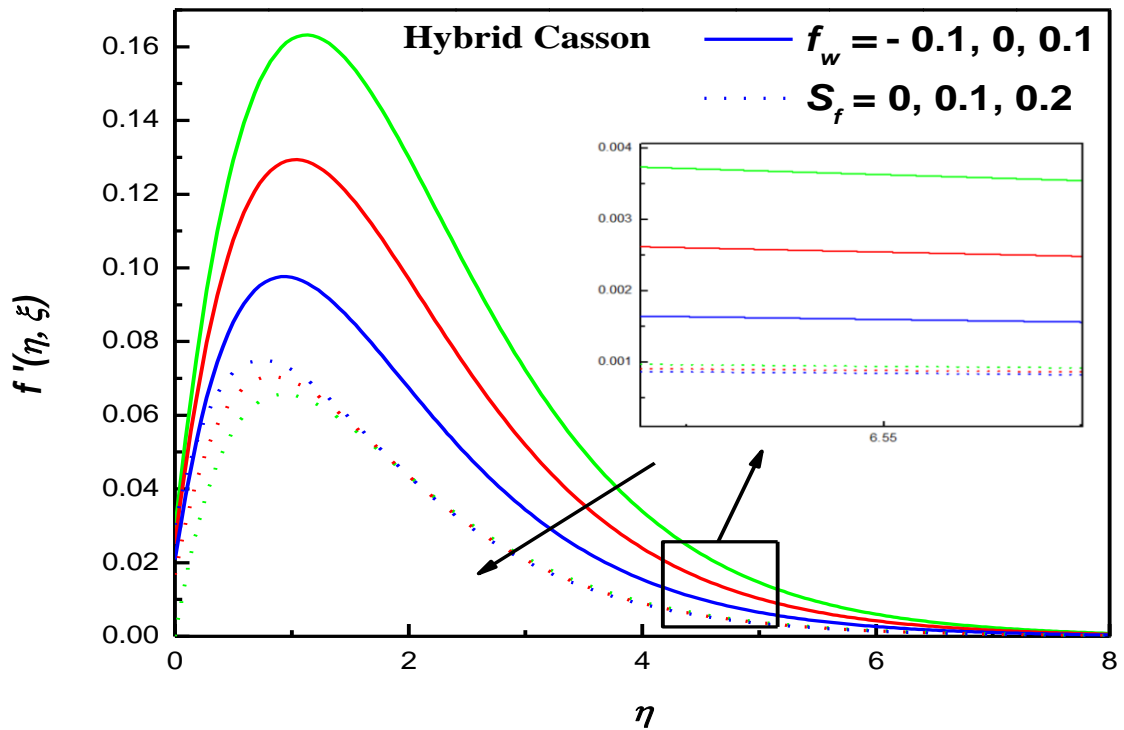


Fig. 11.  $f'(\eta, \xi)$  vs.  $f_w$  and  $S_f$  in Casson case.

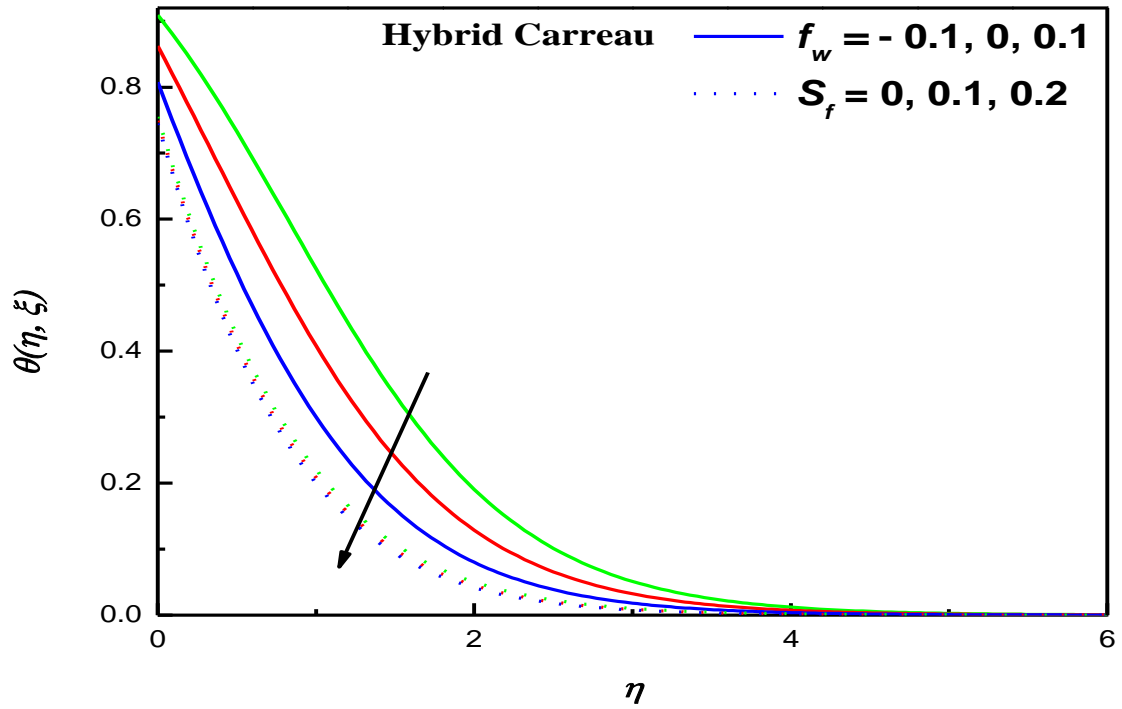


Fig. 12.  $\theta(\eta, \xi)$  vs.  $f_w$  and  $S_f$  in Carreau case.

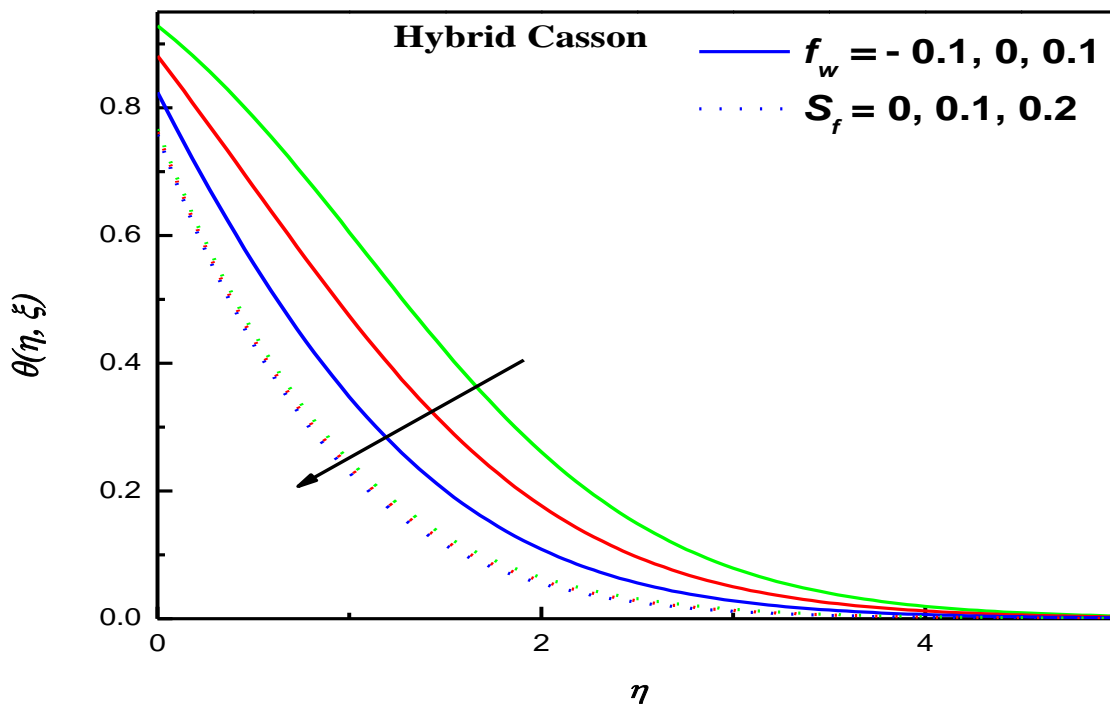


Fig. 13.  $\theta(\eta, \xi)$  vs.  $f_w$  and  $S_f$  in Casson case.

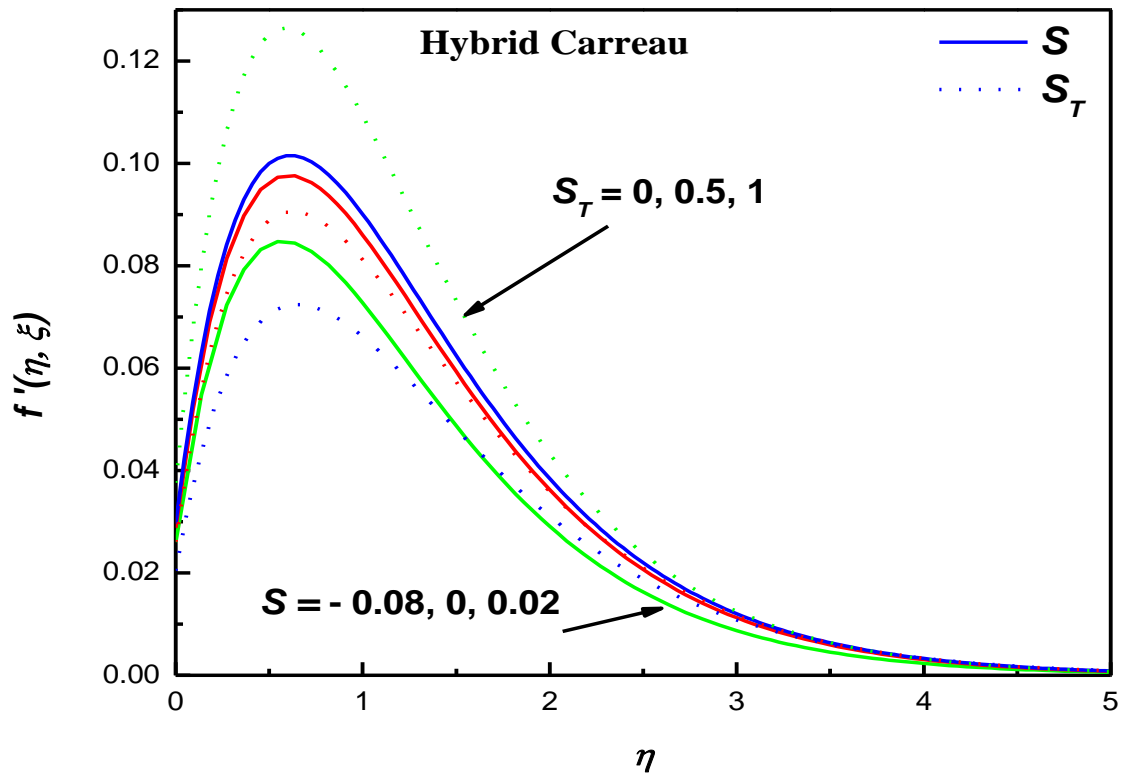


Fig. 14.  $f'(\eta, \xi)$  vs.  $S$  and  $S_T$  in Carreau case.

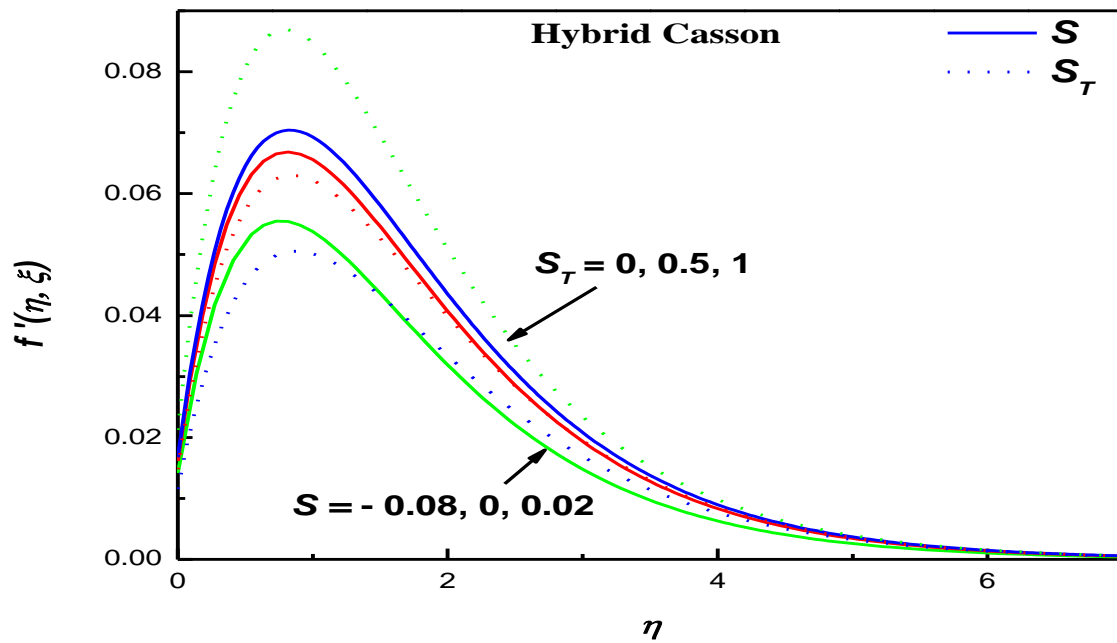


Fig. 15.  $f'(\eta, \xi)$  vs.  $S$  and  $S_T$  in Casson case.

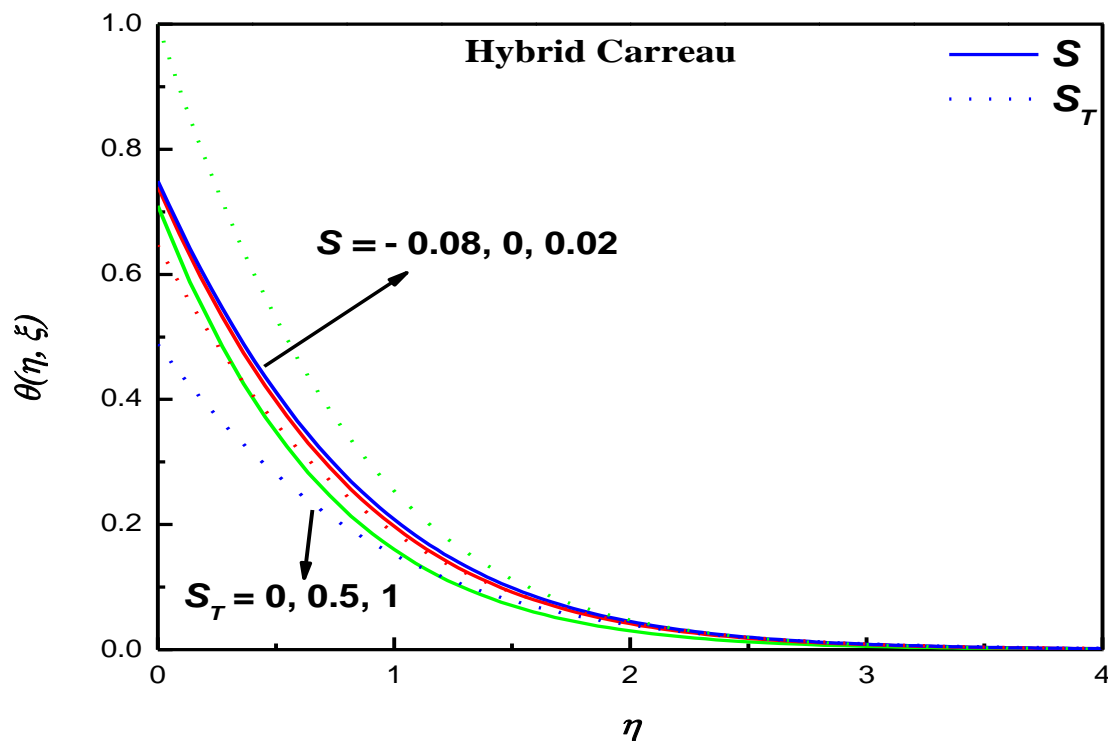


Fig. 16.  $\theta(\eta, \xi)$  vs.  $S$  and  $S_T$  in Carreau case.

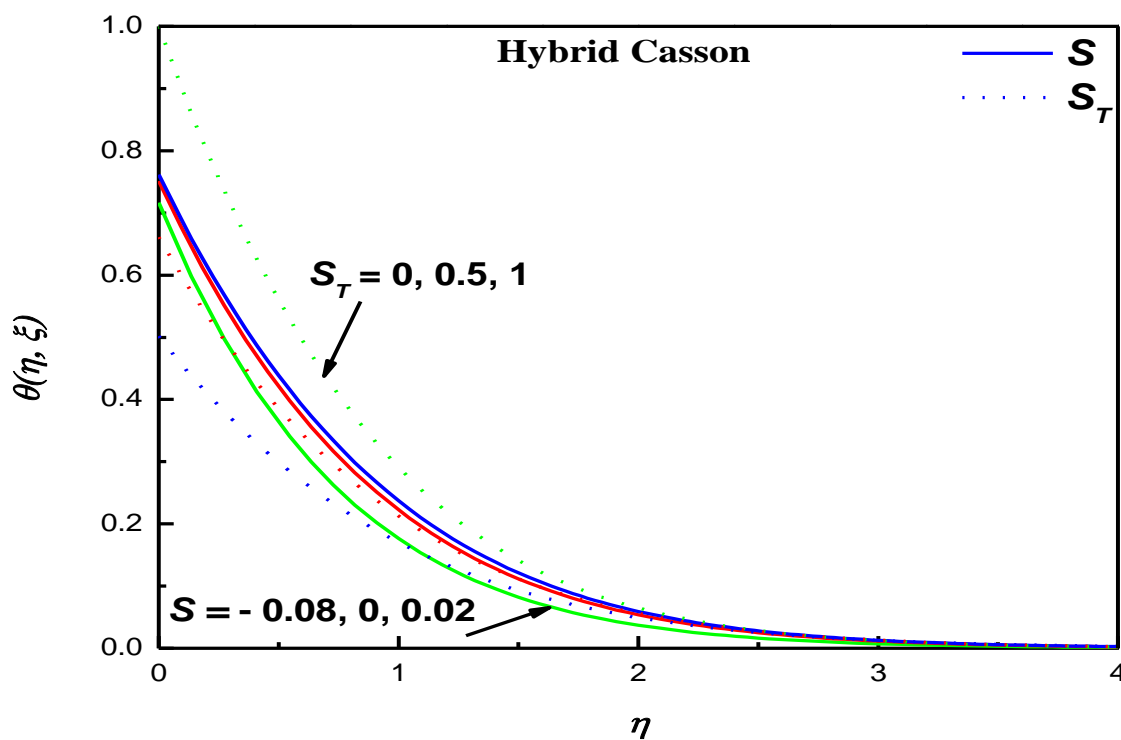


Fig. 17.  $\theta(\eta, \xi)$  vs.  $S$  and  $S_T$  in Casson case.

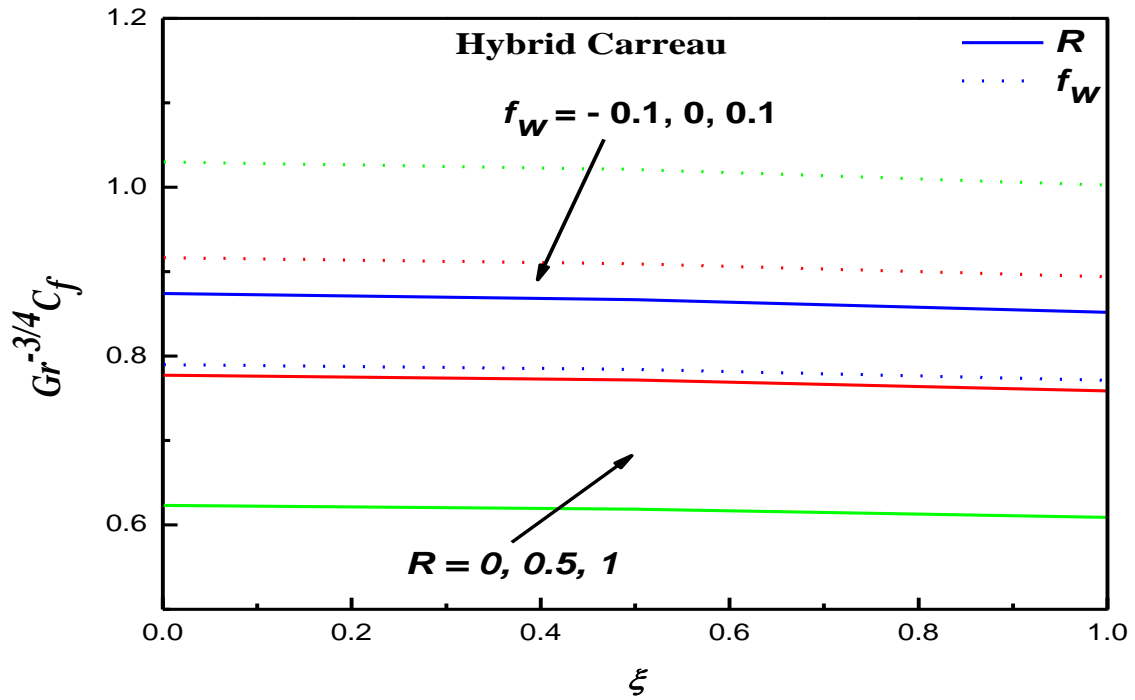


Fig. 18.  $Gr^{-3/4} C_f$  vs.  $\xi$  with  $R$  and  $f_w$  in Carreau case.

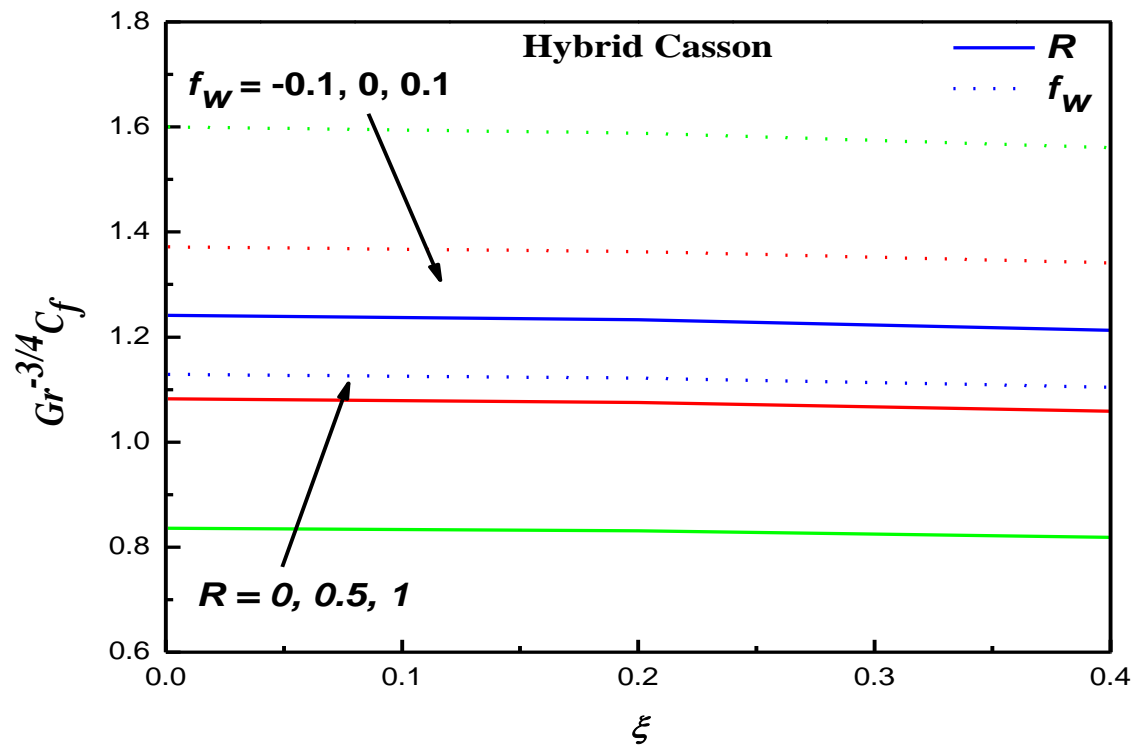


Fig. 19.  $Gr^{-3/4} C_f$  vs.  $\xi$  with  $R$  and  $f_w$  in Casson case.

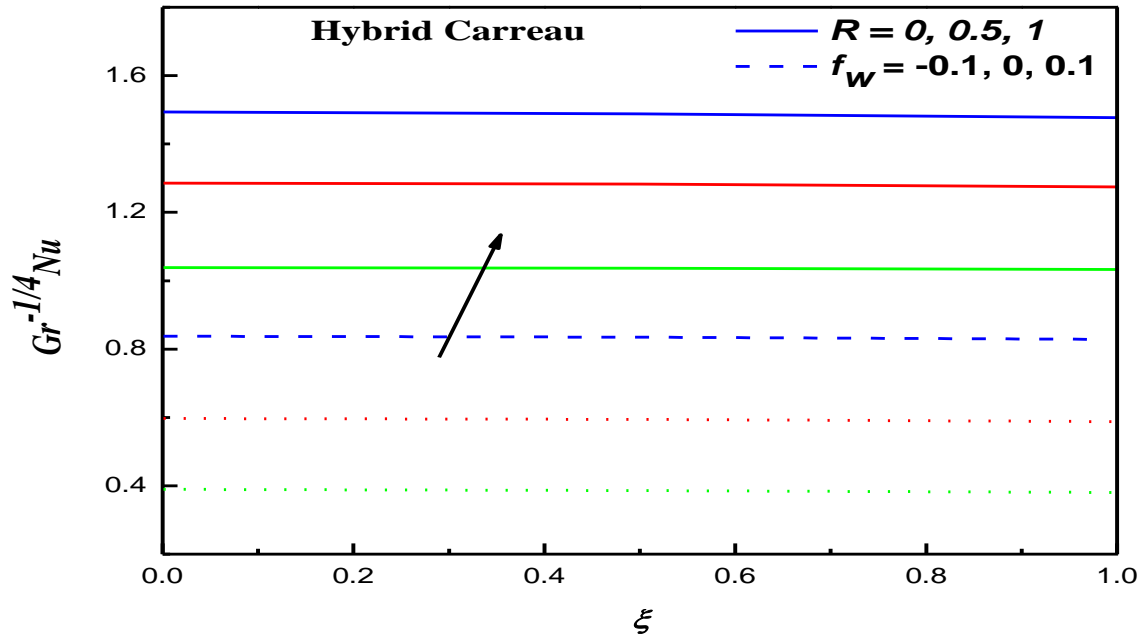


Fig. 20.  $Gr^{-1/4}Nu$  vs.  $\xi$  with  $R$  and  $f_w$  in Carreau case.

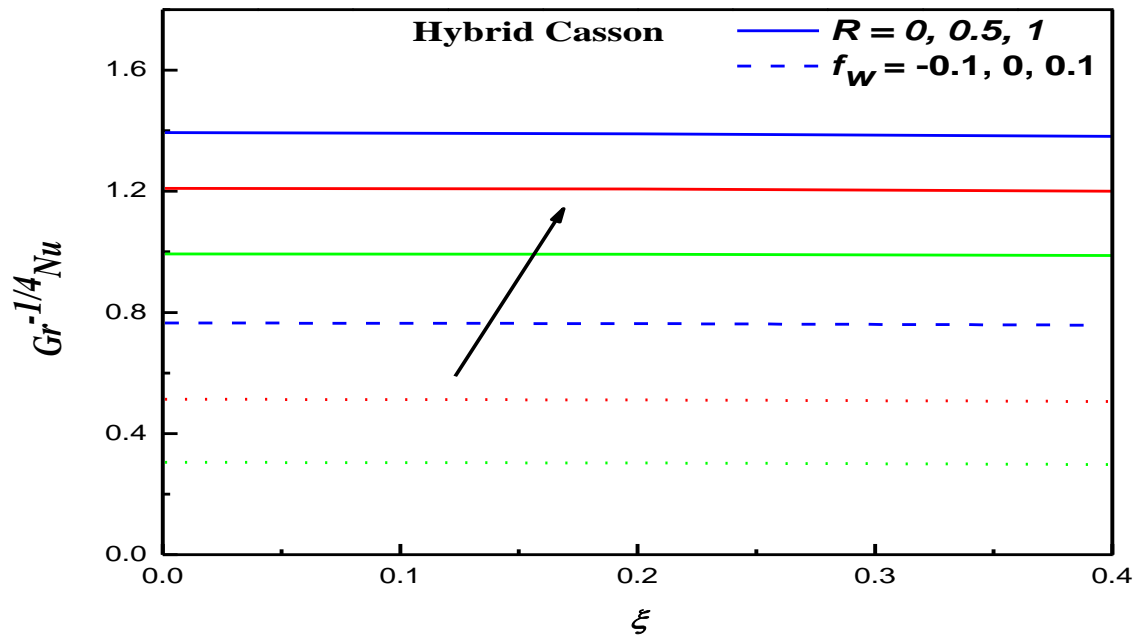


Fig. 21.  $Gr^{-1/4}Nu$  vs.  $\xi$  with  $R$  and  $f_w$  in Casson case.

**Table (1).** Thermo-physical characteristics [27-29].

characteristic	nanoparticles	Used model
$\rho$	$\rho_{nf} = (1 - \varphi_1)\rho_f + \varphi_1\rho_{n_1}$	$\rho_{hnf} = (1 - \varphi_2)[(1 - \varphi_1)\rho_f + \varphi_1\rho_{n_1}] + \varphi_2\rho_{n_2}$
$\rho c_p$	$(\rho c_p)_{nf} = (1 - \varphi_1)(\rho c_p)_f + \varphi_1(\rho c_p)_{n_1}$	$(\rho c_p)_{hnf} = (1 - \varphi_2)[(1 - \varphi_1)(\rho c_p)_f + \varphi_1(\rho c_p)_{n_1}] + \varphi_2(\rho c_p)_{n_2}$
$\mu$	$\mu_{nf} = \frac{\mu_f}{(1 - \varphi_1)^{2.5}}$	$\mu_{hnf} = \frac{\mu_f}{(1 - \varphi_1)^{2.5}(1 - \varphi_2)^{2.5}}$
$k$	$k_{nf} = \frac{k_{n_1} + 2k_f - 2\varphi_1(k_f - k_{n_1})}{k_{n_1} + 2k_f + \varphi_1(k_f - k_{n_1})} \times k_f$	$k_{hnf} = \frac{k_{n_2} + 2k_{nf} - 2\varphi_2(k_{nf} - k_{n_2})}{k_{n_2} + 2k_{nf} + \varphi_2(k_{nf} - k_{n_2})} \times k_{nf}$
$\sigma$	$\sigma_{nf} = 1 + \frac{3\left(\frac{\sigma_{n_1}}{\sigma_f} - 1\right)\varphi_1}{2 + \frac{\sigma_{n_1}}{\sigma_f} - \left(\frac{\sigma_{n_1}}{\sigma_f} - 1\right)\varphi_1} \times \sigma_f$	$\sigma_{hnf} = \frac{\sigma_{n_2} + 2\sigma_{nf} - 2\varphi_2(\sigma_{nf} - \sigma_{n_2})}{\sigma_{n_2} + 2\sigma_{nf} + \varphi_2(\sigma_{nf} - \sigma_{n_2})} \times \sigma_{nf}$
$\beta$	$(\rho\beta)_{nf} = (1 - \varphi_1)(\rho\beta)_f + \varphi_1(\rho\beta)_{n_1}$	$(\rho\beta)_{hnf} = (1 - \varphi_2)[(1 - \varphi_1)(\rho\beta)_f + \varphi_1(\rho\beta)_{n_1}] + \varphi_2(\rho\beta)_{n_2}$

**Table (2).** Thermo-physical characteristics of H<sub>2</sub>O, Al<sub>2</sub>O<sub>3</sub> and Cu.

Characteristic	Water	Alumina	Copper
$c_p(J/kgK)$	4179	765	385
$\rho(kg.m^{-3})$	997.1	3970	8933
$k(W.m^{-1}K^{-1})$	0.613	40	400
$\sigma(S/m)$	0.05	$3.69 \times 10^7$	$5.96 \times 10^7$
$\beta \times 10^{-5}(1/K)$	21	0.85	1.67
$Pr$	6.2		

**Table (3).** Comparison of Nusselt number with Ref. [30], Ref. [31], Ref. [32] and Ref. [33] while  $Pr = 1.0, n = 1, \beta^* \rightarrow \infty$  and  $M = F_r = S_f = S_T = f_w = \varphi_1 = \varphi_2 = 0$ .

$\xi$	$Gr^{-1/4}Nu$				
	Ref. [30]	Ref. [31]	Ref. [32]	Ref. [33]	Present
0	0.4214	0.4216	0.4215	0.4218	0.4220
$\pi/6$	0.4161	0.4163	0.4163	0.4165	0.4165
$\pi/3$	0.4007	0.4006	0.4009	0.4011	0.4003
$\pi/2$	0.3745	0.3741	0.3747	0.3752	0.3758

**Table (4).** Comparison of skin friction coefficient with Ref. [28], Ref. [29], Ref. [30] and Ref. [30] while  $Pr = 1.0$ ,  $n = 1$ ,  $\beta^* \rightarrow \infty$  and  $M = F_r = S_f = S_T = f_w = \varphi_1 = \varphi_2 = 0$ .

$\xi$	$Gr^{-3/4}C_f$				
	Ref. [30]	Ref. [31]	Ref. [32]	Ref. [33]	Present
0	0.0000	0.0000	0.0000	0.0000	0.0000
$\pi/6$	0.4151	0.4139	0.4150	0.4247	0.4124
$\pi/3$	0.7558	0.7527	0.7557	0.7559	0.7530
$\pi/2$	0.9579	0.9526	0.9578	0.9576	0.9583
$2\pi/3$	0.9756	0.9677	0.9555	0.9551	0.9766

**Table (5).** The various values of  $Gr^{-3/4}C_f$  and  $Gr^{-1/4}Nu$  for diverse values of  $\varphi_1, \varphi_2, S_T, F_r, R$  and  $f_w$  when  $M = 2.0, Pr = 6.2, S_f = 0.1, S = 0.02$  and  $K = 1$ .

$\varphi_1$	$\varphi_2$	$S_T$	$F_r$	$R$	$f_w$	Carreau		Casson	
						$Gr^{-3/4}C_f$	$Gr^{-1/4}Nu$	$Gr^{-3/4}C_f$	$Gr^{-1/4}Nu$
0	0.04	0.3	1.0	0.1	0.2	0.1120	1.0200	0.1455	0.9931
0.01						0.1130	1.0246	0.1470	0.9974
0.02						0.1140	1.0290	0.1485	1.0014
0.03						0.1149	1.0331	0.1500	1.0053
	0.02					0.1117	1.0220	0.1454	0.9949
	0.05					0.1165	1.0384	0.1522	1.0103
		0.0				0.1466	1.3885	0.1906	1.3335
		0.2				0.1248	1.1320	0.1629	1.0977
		0.4				0.1093	0.9599	0.1430	0.9365
			0			0.1096	0.9606	0.1432	0.9369
			2			0.1090	0.9593	0.1427	0.9361
			4			0.1084	0.9580	0.1422	0.9353
				0		0.1029	0.9196	0.1341	0.8997
				0.4		0.1214	1.0621	0.1616	1.0326
				0.8		0.1335	1.1853	0.1799	1.1489
					-0.2	0.1821	0.2293	0.2691	0.1895
					0.2	0.1335	1.1853	0.1799	1.1489
					0.4	0.1036	1.7537	0.1323	1.7343

**Conflict of interest**

The authors declare that there is no conflict of interest.

**References**

[1] - N. Casson, A flow equation for the pigment oil suspensions of the printing ink type, In: Mill, C.C., Ed., Rheology of Disperse Systems, Pergamon Press, Oxford. (1959) 84-104.  
 [2] - H.R. Kataria, A.S. Mittal, Velocity, mass and temperature analysis of gravity-driven convection nanofluid flow past an oscillating vertical plate in the presence of magnetic field in a porous medium, Appl. Therm. Eng. 110

- (2017) 864-874. <https://doi.org/10.1016/j.applthermaleng.2016.08.129>.
- [3] - K.V.B. Rajakumar, K.S. Balamurugan, M. Umasankar, C.V. Murthy, Radiation, dissipation and Dufour effects on MHD free convection Casson fluid flow through a vertical oscillatory porous plate with ion-slip current, *Int. J. Heat. Technol.* 36 (2018) 494-508. <https://doi.org/10.18280/ijht.360214>.
- [4] - G.S. Seth, R. Kumar, R. Tripathi, A. Bhattacharyya, Double diffusive MHD Casson fluid flow in a non-Darcy porous medium with Newtonian heating and thermo-diffusion effects. *Int. J. Heat Technol.* 36(4) (2019) 1517. <https://doi.org/10.18280/ijht.360446>.
- [5] - A.S. Mittal, H.R. Patel, Influence of thermophoresis and Brownian motion on mixed convection two dimensional MHD Casson fluid flow with non-linear radiation and heat generation, *Phys. A.* 537 (2020) 122710. <https://doi.org/10.1016/j.physa.2019.122710>.
- [6] - E.R. El-Zahar, A. Mahdy, A.M. Rashad, W. Saad, L.F. Seddek, Unsteady MHD mixed convection flow of non-Newtonian Casson hybrid nanofluid in the stagnation zone of sphere spinning impulsively, *fluids.* 6(6) (2021) 197. <https://doi.org/10.3390/fluids6060197>.
- [7] - S. Akram, Effects of nanofluid on peristaltic flow of a Carreau fluid model in an inclined magnetic field, *Heat Transf.* 43 (2014) 368-383. <https://doi.org/10.1002/htj.21082>.
- [8] - T. Hayat, R. Iqbal, A. Tanveer, A. Alsaedi, Mixed convective peristaltic transport of Carreau–Yasuda nanofluid in a tapered asymmetric channel, *J. Mol. Liq.,* 223 (2016) 1100-1113. <https://doi.org/10.1016/j.molliq.2016.08.003>.
- [9] - K. Vajravelu, S. Sreenadh, R. Saravana, Combined influence of velocity slip, temperature and concentration jump conditions on MHD peristaltic transport of a Carreau fluid in a non-uniform channel, *Appl. Math. Comput.* 225 (2013) 656-676. <https://doi.org/10.1016/j.amc.2013.10.014>.
- [10] - M. Kothandapani, J. Prakash, S. Srinivas, Peristaltic transport of a MHD Carreau fluid in a tapered asymmetric channel with permeable walls, *Int. J. BioMath.,* 8 (2015) 1550054. <https://doi.org/10.1142/S1793524515500540>.
- [11] - A.S. Hamarshah, F.A. Alwawi, H.T. Alkasasbeh, A.M. Rashad, R. Idris, Heat transfer improvement in MHD natural convection flow of graphite oxide/carbon nanotubes-methanol based casson nanofluids past a horizontal circular cylinder, *Processes,* 8(11) (2020) 1444. <https://doi.org/10.3390/pr8111444>.
- [12] - E.R. El-Zahar, A.M. Rashad, L.F. Seddek, Impacts of viscous dissipation and brownian motion on Jeffrey nanofluid flow over an unsteady stretching surface with thermophoresis, *Symmetry.* 12(9) (2020) 1450. <https://doi.org/10.3390/sym12091450>.
- [13] - M.A. Abdelhafez, A. Awad, M.A. Nafe, D.A. Eisa, Time-dependent viscous flow of higher-order reactive MHD Maxwell nanofluid with Joule heating in a porous regime, *Wave Random Complex.* (2021). <https://doi.org/10.1080/17455030.2021.1927237>.
- [14] - S.R.R. Reddy, P.B.A. Reddy, A.M. Rashad, Effectiveness of binary chemical reaction on magneto-fluid flow with Cattaneo–Christov heat flux model, *Proc. Inst. Mech. Eng. C J. Mech. Eng. Sci.* 235(12) (2021) 2192-2200. <https://doi.org/10.1177/0954406220950347>.
- [15] - S. Jakeer, P.B.A. Reddy, A.M. Rashad, H.A. Nabwey, Impact of heated obstacle position on magneto-hybrid nanofluid flow in a lid-driven porous cavity with Cattaneo-Christov heat flux pattern, *Alex. Eng. J.* 60(1) (2021) 821-835. <https://doi.org/10.1016/j.aej.2020.10.011>.
- [16] - S. EL-Kabeir, A.M. Rashad, W. Khan, Z.M. Abdelrahman, Micropolar ferrofluid flow via natural convective about a radiative isoflux sphere, *Adv. Mech. Eng.* 13(2) (2021) 1687814021994392. <https://doi.org/10.1177/1687814021994392>.
- [17] - H.R. Kataria, A.S. Mittal, Mathematical model for velocity and temperature of gravity-driven convective optically thick nanofluid flow past an oscillating vertical plate in presence of magnetic field and radiation, *J. Niger. Math. Soc.* 34(3) (2015) 303. <https://doi.org/10.1016/j.jnnms.2015.08.005>.
- [18] - K. Raghunath, R. Sivaprasad, G.S.S. Raju, Heat and mass transfer on MHD flow of non-Newtonian fluid over an infinite vertical porous plate, *Int. J. Appl. Eng. Res.* 13(13) (2018) 11156- 11163.
- [19] - A.j. Chamkha, T. Armaghani, M.A. Mansour, A.M. Rashad, H. Kargarsharifabad, MHD convection of an  $Al_2O_3$ -Cu/water hybrid nanofluid in an inclined porous cavity with internal heat generation/absorption, *I. J. C. C. E.* (2021). <https://doi.org/10.30492/IJCCE.2021.136201.4328>.
- [20] - M. Obulesu, K. Raghunath, R. Sivaprasad, Hall current effects on MHD convective flow past a porous plate with

- thermal radiation, chemical reaction with radiation absorption, *AIP Conf. Proc.* 2245 (2020) 020003. <https://doi.org/10.1063/5.0014423>.
- [21] - M.A. Mansour, R.S. Gorla, S. Siddiqua, A.M. Rashad, T. Salah, Unsteady MHD natural convection flow of a nanofluid inside an inclined square cavity containing a heated circular obstacle, *Int. J. Nonlinear Sci.* (2021). <https://doi.org/10.1515/ijnsns-2020-0138>.
- [22] - M.A. Abdelhafez, A.A. Awad, M.A. Nafe, D.A. Eisa, Flow of mixed convection for radiative and magnetic hybrid nanofluid in a porous material with Joule heating, *Heat Transf.* 51 (2021) 2995-3017. <https://doi.org/10.1002/htj.22433>.
- [23] - M.A. Abdelhafez, A.A. Awad, M.A. Nafe, D.A. Eisa, Effects of yield stress and chemical reaction on magnetic two-phase nanofluid flow in a porous regime with thermal ray, *Indian J. Phys.* 96 (2022) 3579–3589. <https://doi.org/10.1007/s12648-022-02288-1>.
- [24] - A.S. Rao, N. Nagendra, C.H. Amanulla, M. Reddy, O.A. Beg, Computational analysis of non-Newtonian boundary layer flow of nanofluid past a vertical plate with partial slip, *M. M. C. B.* 86(1) (2017) 271.
- [25] - N. Nagendra, C.H. Amanulla, M.S. Reddy, Slip effects on MHD flow of a Williamson fluid from an isothermal sphere: a numerical study, *M. M. C. B.* 86(3) (2017) 782-807. [https://doi.org/10.18280/mmc\\_b.860311](https://doi.org/10.18280/mmc_b.860311)
- [26] - T. Salahuddin, Carreau fluid model towards a stretching cylinder: using Keller box and shooting method, *Ain Shams Eng. J.* 11 (2020) 495. <https://doi.org/10.1016/j.asej.2017.03.016>.
- [27] - M.A. Rashad, M.A. Nafe, D.A. Eisa, Heat variation on MHD Williamson hybrid nanofluid flow with convective boundary condition and Ohmic heating in a porous material, *Sci. Rep.* 13 (2023) 6071. <https://doi.org/10.1038/s41598-023-33043-z>.
- [28] - M.A. Rashad, M.A. Nafe, D.A. Eisa, Variation of thermal conductivity and heat on magnetic Maxwell hybrid nanofluid viscous flow in a porous system with higher order chemical react, *Spec. Top. Rev.* 14(2) (2023) 17-32. <https://doi.org/10.1615/SpecialTopicsRevPorousMedia.2023045731>.
- [29] - M.A. Rashad, M.A. Nafe, D.A. Eisa, Heat generation and thermal radiation impacts on flow of magnetic Eyring–Powell hybrid nanofluid in a porous medium, *Arab. J. Sci. Eng.* 48, (2023) 939–952. <https://doi.org/10.1007/s13369-022-07210-9>.
- [30] - Merkin, Free convection boundary layer on an isothermal horizontal circular cylinder, *ASME/AICHE, Heat Transfer Conference*, St. Louis, Mo., U.S.A. (1976) 9.
- [31] - M.M. Molla, S.C. Saha, M.A.I. Khan, M.A.Hossain, Radiation effects on natural convection laminar flow from a horizontal circular cylinder, *Desalination Water Treat.* 30(1-3) (2011) 89-97. <https://doi.org/10.5004/dwt.2011.1870>.
- [32] - T. Javed, A. Majeed, I. Mustafa, MHD effects on natural convection laminar flow from a horizontal circular cylinder in presence of radiation, *Rev. Mex. Fis.* 61 (2015) 450.
- [33] - N. Nagendra, B. Venkateswarlu, Z. Boulahia, C. Amanulla, G.K. Ramesh, Magneto Casson-Carreau Fluid Flow through a Circular Porous Cylinder with Partial Slip, *J. Appl. Comput. Mech.* (2021) 1. <https://doi.org/10.22055/JACM.2021.38390.3215>.